ChemPubSoc Europe

DOI: 10.1002/cphc.201800592

CHEMPHYSCHEM Articles

Genesis of $MgCl_2$-based Ziegler-Natta Catalysts as Probed with Operando Spectroscopy

Alessandro Piovano,[a] Paul Pletcher,[b] Marjolein E. Z. Velthoen,[b] Silvia Zanoni,[b] Sang-Ho Chung,[b, c] Koen Bossers,[b] Maarten K. Jongkind,[b] Gianluca Fiore,[a] Elena Groppo,*[a] and Bert M. Weckhuysen*[b]

Ziegler-Natta catalysts for olefin polymerization are intrinsically complex multi-component systems. The genesis of the active sites involves several simultaneous and sequential steps, making the individual steps and interconnections difficult to be unraveled in an unambiguous manner. In this work, we combine X-ray diffraction and spectroscopy to probe each step of the birth and life of a $MgCl_2$-based Ziegler-Natta catalyst, namely the formation of high surface area $MgCl_2$ by dealcoholation of an alcoholate precursor, the $TiCl_4$ grafting, and the subsequent activation by triethylaluminum as co-catalyst. The so-prepared catalyst was tested towards ethylene polymerization, leading to the production of mainly crystalline high-density polyethylene. The use of *operando* characterization techniques allowed probing the transient details that are difficult to be dissected in the aftermath, but can radically affect the overall catalytic process.

1. Introduction

Nowadays, *operando* spectroscopic techniques are becoming a mature technology to gain fundamental knowledge at the molecular level of the catalytic reactions taking place under industrially relevant conditions, which include gas or liquid phase conditions, reactions in the presence of solvents, at high temperatures and pressures.[1–8] Notable examples can be found in recent literature about some industrial catalytic systems that were implemented thanks to the know-how derived from the *operando* spectroscopic approach. For instance, *operando* spectroscopy helped in understanding and facing the deactivation of some hydrogenation catalysts by CO_2 as byproduct,[9] in defining the operating potentials necessary to replace platinum with iron into the oxygen reduction reaction (ORR) catalysts,[10] and in improving the recyclability of the selective catalytic reduction (SCR) catalysts by identifying the side reactions responsible for hydrothermal aging.[11] In each of these cases and in many others, the use of *operando* spectroscopic techniques rationally resolved the important technical problems that were compromising the effectiveness of the catalytic processes.

In contrast, olefin polymerization catalysts, in particular the Ziegler-Natta catalysts, have not been the topic of interest in *operando* spectroscopic studies yet, despite their tremendous impact in modern chemical industry.[12–15] The high dilution and the intrinsic heterogeneity of the catalytic sites, the co-presence of spectator species and the high air sensitivity of the catalysts and their activators are among the main reasons for the lack of Ziegler-Natta *operando* spectroscopic studies.[16] For these reasons, despite sixty years of industrial practice, the structural and electronic properties of the active sites and their functioning during the olefin polymerization reaction are still subject of debate,[17–23] and most of the advances in this field are still based on a trial and error approach.[24,25] Recently, *operando* spectroscopies were successfully applied to disclose the genesis of the Cr active sites in the Cr^{VI}/SiO_2 Phillips catalyst[26] and the molecular-level properties of Phillips-type catalysts modified by aluminum-alkyls,[26–28] demonstrating that these methods have progressed enough to meet the technical challenges posed by olefin polymerization catalysts. This stimulated us in applying the same ensemble of characterization techniques to investigate the genesis of the active sites for the $MgCl_2$-supported Ziegler-Natta catalysts, the topic of this work.

Generally speaking, Ziegler-Natta catalysts are multi-component systems, whose synthesis involves several steps directly inside the reactor, through the sequential addition of different building blocks onto the support material.[29,30] As far as the $MgCl_2$ support is concerned, its introduction to the composition of Ziegler-Natta catalysts in the 1970s marked the beginning of the so called third generation of catalysts and the consequent exponential increase of the polyolefins world production.[29–31] Historically, the reason for the success of $MgCl_2$ as a dispersing phase for $TiCl_x$ was explained on account of the similarity between its crystalline structure and that of the α and γ phases

[a] *Dr. A. Piovano, Dr. G. Fiore, Prof. E. Groppo*
Department of Chemistry, INSTM and NIS Centre
University of Torino
Via Quarello 15A, 10135 Torino (Italy)
E-mail: elena.groppo@unito.it
[b] *Dr. P. Pletcher, M. E. Z. Velthoen, S. Zanoni, Dr. S.-H. Chung, K. Bossers, M. K. Jongkind, Prof. B. M. Weckhuysen*
Inorganic Chemistry and Catalysis Group
Debye Institute for Nanomaterials Science
Utrecht University
Universiteitsweg 99, 3584 CG Utrecht (The Netherlands)
E-mail: b.m.weckhuysen@uu.nl
[c] *Dr. S.-H. Chung*
Van 't Hoff Institute for Molecular Sciences (HIMS)
University of Amsterdam
PO Box 94157, 1090 GD Amsterdam (The Netherlands)

of $TiCl_3$, which were the main constituents in the previous generations of catalysts.[32–34] However, this concept progressively evolved simultaneously with the discovery of the active role of $MgCl_2$ in the olefin polymerization process. Indeed, the exposed $MgCl_2$ surfaces affect the stereo- and electro-chemical properties of the grafted $TiCl_x$ species, thus influencing the stereo-regularity of the obtained polypropylene,[35–37] the molecular weight distribution[38,39] and the particles morphology[40,41] of several polymers, as well as the co-polymerization behavior of different monomers,[42] approaching the same relevance as the ancillary ligands in homogeneous catalysis.[43]

Within this context, the $MgCl_2$ pre-treatment plays a dominant role in determining the specific surface area of the material and the morphology of the nanocrystals (i.e. the main exposed surfaces). As a matter of fact, the distribution of the active phase has already been proved to depend on the relative extent of the surfaces exposing either 4-fold coordinated Mg^{2+} sites, as the (110) surface, or 5-fold coordinated Mg^{2+} sites, as the (104) one.[44,45] In the industrial practice, several procedures are adopted to produced $MgCl_2$-based materials, including the mechanical ball-milling of $MgCl_2$ in the co-presence of $TiCl_4$ and suitable electron donors, the decomposition of previously synthesized adducts between $MgCl_2$ and Lewis bases (such as alcohols or ethers) in the presence of $TiCl_4$, and the direct chlorination of Mg and Ti alkoxides with AlR_nCl_{3-n} compounds.[32,46–55] The latter method was recently proved to promote the formation of $MgCl_2$ nanocrystals whose morphologies depend on the starting alcoholic adduct.[45,56–60] In the past, Thune and coworkers monitored by FT-IR spectroscopy in ATR mode the direct transformation of the alcoholate precursor into the Ziegler-Natta pre-catalyst in the presence of $TiCl_4$ and an electron donor.[61]

Complementary information about the chemically activated $MgCl_2$ material can be achieved through a detailed investigation of the complete thermal dealcoholation process. Such a procedure is quite unusual in the industrial practice, but it is fundamental to unravel the whole sequence of chemical reactions taking place during the formation of the $MgCl_2$ support material, affecting its final properties. So far, most of the research efforts in this sense have been mainly focused on the synthesis and the static analysis of a series of $MgCl_2$-nROH adducts (where ROH is usually ethanol) with different stoichiometry, mimicking the progressive dealcoholation by decreasing the n value from 6 to 0. Among the most relevant studies, we cite the pioneering work of Di Noto et al. reporting a detailed XRD and FT-IR characterization of several $MgCl_2$-nEtOH adducts,[62] followed by the Raman spectroscopic investigation of Tewell et al.,[63] the particle size distribution analysis of Ye et al.,[64] and the NMR structural characterization of Sozzani et al., who first proposed also an analytical methodology to recognize the pure $MgCl_2$-nEtOH compounds within a mixture.[65] All of these works agree in identifying $n \approx 2$ as the stoichiometric value that separates the compounds containing Mg atoms octahedrally coordinated to the oxygen atoms of ethanol ($n > 2$) from those in which a ionic structure is already recognizable ($n < 2$). For this reason, D'Anna et al. adopted exactly the $MgCl_2$-2EtOH adduct as the model system to study the successive titanation step and the structure of the Ziegler-Natta pre-catalysts.[66] All these studies represent a fundamental benchmark for investigating the formation of $MgCl_2$ from alcoholate precursors, though the industrial situation is complicated by the co-presence of several intermediate states. In this sense, the works of Bart and Roovers and of Jalali Dil et al.[67,68] are much closer to the industrial scenario. The former reports an ex situ XRD study on the adducts obtained upon step-by-step dealcoholation of $MgCl_2$-6EtOH performed in accordance with thermogravimetric analysis (TGA), pointing out the co-presence of several metastable intermediate phases at each step. Three main structures were described: structures with only discrete mononuclear species (either ionic or covalent), polymeric polynuclear structures resulting from the association of mixed $Mg(EtOH)_nCl_{(6-n)}$ octahedra (with the Cl ligands as bridges), and more complex polynuclear structures with an intermediate stoichiometry.[67] Jalali Dil et al. reported a scanning electron microscopy (SEM) investigation of some differently dealcoholated $MgCl_2$ materials and of the polypropylene produced by the corresponding $MgCl_2$-supported Ziegler-Natta catalysts. It was found that the porosity of the $MgCl_2$ progressively increases upon decreasing the alcohol content, and consequently the polymer morphology changes from eggshell to porous with an internal network.[68]

As far as the active phase is concerned, it is generally constituted by $TiCl_4$ as a precursor, which is then activated by the co-catalyst, typically an Al-alkyl. The most used Ziegler-Natta co-catalyst is triethylaluminum (TEA), although several other organo-aluminum compounds can be used to vary the electronic properties and the catalytic activity of the metal centers. The activator is an integral part of the active phase, and significantly influences the activity and the stability of the catalyst, the polymerization kinetic profile, and the polymer molecular weight and stereoregularity.[21,69] The reaction between the Ti^{4+} chloride species on the pre-catalyst surface and the Al-alkyl compound is generally described as constituted by two steps: the formation of an organo-bimetallic complex and its dissociation, with the concurrent reduction of Ti^{4+} to Ti^{3+} and the exchange of a Cl ligand with an alkyl group in the coordination sphere of the titanium.[70] Further reduction to Ti^{2+} is normally prevented because of the steric hindrance of the surrounding chlorinated Al-alkyl byproducts,[70] although it is possible in the presence of a very large excess of AlR_3. In such a case, the role of the Ti^{2+} species in olefin polymerization is still controversial and strongly depends on the catalytic process considered.[71–75] Despite some theoretical studies about the energy barriers and the thermodynamic stability of the intermediate species within the redox circuit including the Ti^{4+} precursor, the active Ti^{3+}, and the deactivated over-reduced Ti^{2+},[70,76] the scientific community is still looking for an experimental evidence that could shed light on the activation mechanism at the molecular level.

The present work aims at sequentially characterizing the steps that lead to the genesis of the active sites in a Ziegler-Natta catalyst by employing complementary spectroscopic methods, in order to identify the transient intermediate species. This represents a fundamental step towards the elucidation of

the relationship between structure and performances.[77] As a part of this investigation, we studied the thermal dealcoholation of $MgCl_2$-ROH adducts into high surface area $MgCl_2$. It is worth remarking that such a process does not necessarily pass through a sequence of compounds with well-defined stoichiometry, conversely to those characterized in the above-mentioned works. To the best of our knowledge this is the first attempt to monitor with an *operando* multi-technique approach the evolution of the $MgCl_2$-nROH adducts to $MgCl_2$. Two different alcoholate adducts were considered as precursors: $MgCl_2$-nMeOH and $MgCl_2$-nEtOH. While the former was recently demonstrated by Thushara et al. to generate the most suitable $MgCl_2$ material for a surface science investigation in terms of specific surface area, nanoparticles morphology and distribution of the catalytic sites,[45,59] the results obtained starting from the ethanol adduct serve as an indispensable connection with previous literature. Similarities and differences between the two cases are duly pointed out in the text. Afterwards, the investigation is focused on the Ti species, which are the catalytically relevant active sites. In particular, we report some direct observations on the $TiCl_4$ grafting on the $MgCl_2$ surfaces, the reaction with the TEA activator, and the activity towards ethylene polymerization.

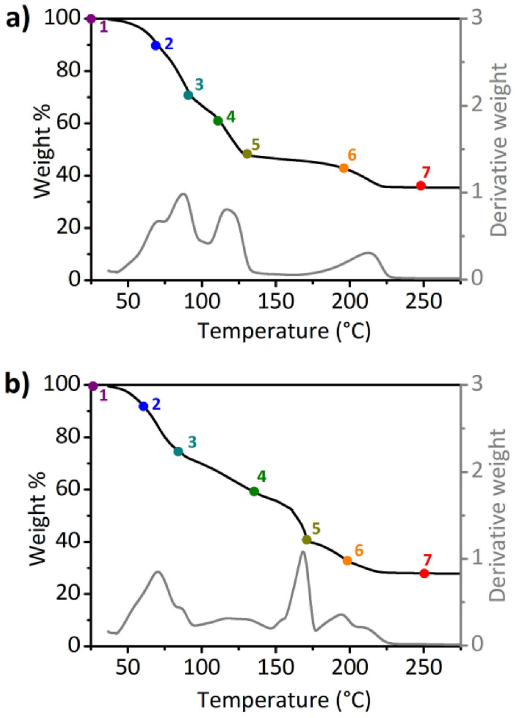

Figure 1. Thermogravimetric (black line) and differential thermogravimetric (grey line) analysis of $MgCl_2$-6MeOH (part a) and $MgCl_2$-6EtOH (part b) under N_2 flux (50 mL/min), collected at a heating ramp of 2 °C/min. The colored dots delimit the temperature steps corresponding to the loss of one alcohol molecule. These steps have been taken as references for the successive measurements.

2. Results and Discussion

2.1. Synthesis of High-surface-area $MgCl_2$ from $MgCl_2$-nROH Adducts

Figure 1 shows the thermogravimetric analysis (TGA) conducted on the $MgCl_2$-nROH adducts. In both cases, a systematic and gradual loss of alcohol molecules occurs throughout the whole temperature range from 25 °C to 250 °C, as evidenced by the presence of sharp and quite well-defined peaks in the derivative curve.

In the case of the adduct with methanol (part a), the total weight loss observed at the end of the dealcoholation process (67%) is in excellent agreement with the one calculated on the basis of a starting $MgCl_2$-6MeOH stoichiometry, within an error of ±2%.[78] Besides, a more refined analysis of the TGA profile revealed that, although the weight loss begins already at room temperature, the first methanol molecule is completely lost only around 70 °C, and that almost five out of the six alcohol molecules are lost below 150 °C. Comparable results were obtained from the TGA of the adduct with ethanol (part b). Indeed, also in the latter case the complete dealcoholation is achieved at 250 °C and the observed total weight loss (73%) is compatible with an initial $MgCl_2$-6EtOH stoichiometry. The main difference is that the $MgCl_2$-6EtOH adduct loses only four out of the six ligands below 150 °C, in agreement with previously published data,[65] possibly due to the lower volatility of ethanol with respect to methanol.

The $MgCl_2$-ROH dealcoholation process was successively followed by means of structural (XRPD) and spectroscopic (DR UV-Vis and DRIFT) methods under *operando* conditions. For each adduct we have defined six temperature steps, corresponding to the most relevant weight losses as determined by TGA (colored dots in Figure 1), at which we have been collecting XRPD patterns and DR UV-Vis spectra, while the DRIFT spectra were collected continuously during the temperature ramp.

Figure 2 shows the evolution of the XRPD patterns during the dealcoholation of the $MgCl_2$-6ROH adducts under N_2 flow at increasing temperatures. In the case of $MgCl_2$-6MeOH (part a), pattern 1, collected at room temperature, is characteristic of a solid solution in which both the Mg^{2+} cations and the Cl^- anions are surrounded by six alcohol molecules in the first solvation shell,[79,80] thus confirming the stoichiometry resulting from the TGA. In this sense, the structure of the solid $MgCl_2$-6MeOH adduct can be considered as an arrangement of discrete octahedra with Mg^{2+} ions in the centers and MeOH molecules in the corners, and with the chloride ions excluded from the Mg^{2+} coordination sphere as counterions.[81] Upon increasing the temperature, the appearance, transformation and disappearance of several (broad) diffraction peaks are clearly evident and testify the formation of different intermediate crystalline phases as a function of the alcohol content. In particular, the disappearance of the two peaks at 19° and 21° (triangles in Figure 2a) and the appearance of a very weak peak at 12.5° in pattern 4 (star in Figure 2a) are associated with the transition from predominantly solvated ionic structures to covalent $MgCl_2$ long chains, featuring chlorine bridges connecting the Mg atoms.[62,82] The final XRPD pattern (pattern 7) is that

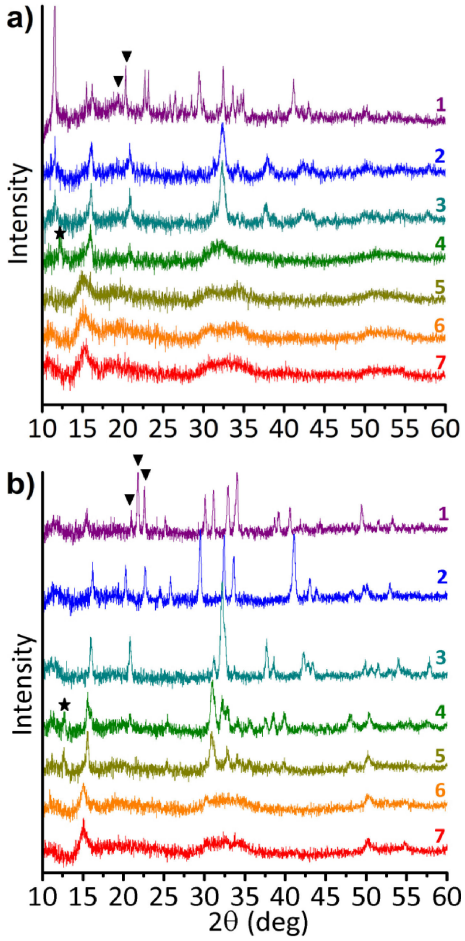

Figure 2. Evolution of the X-ray powder diffraction (XRPD) patterns upon dealcoholation of $MgCl_2$-6MeOH (part a) and $MgCl_2$-EtOH (part b), under N_2 flux (20 mL/min) at increasing temperatures (2 °C/min), from 25 to 250 °C. The color code is the same as in Figure 1 (25, 60, 90, 120, 150, 200 and 250 °C for $MgCl_2$-MeOH, and 25, 50, 80, 120, 170, 200 and 250 °C for $MgCl_2$-EtOH).

of a layered δ-$MgCl_2$ phase characterized by an extensive structural disorder, in agreement with the literature findings,[83,84] although the sporadic alternation of only partially converted MgCl(OMe) layers cannot be excluded.[60] In particular, the diffraction peak around $2\theta = 15°$ ($d = 5.90$ Å) corresponds to the (001) basal plane, and its broadness is related to the nano-sized dimensions of the crystalline domains. Moreover, very broad and weak peaks at 2θ values around 30–35° and 50° indicate the presence of the catalytically relevant (104) and (110) planes, respectively.[85] For the $MgCl_2$-6EtOH sample, a slower evolution of the XRPD patterns is observed (Figure 2b). The diffraction peaks associated with the intermediate crystalline phases disappear at higher temperatures, in fair agreement with the thermogravimetric profile (Figure 1b). However, the final pattern is the same as that obtained from $MgCl_2$-6MeOH. This is a clear limit of the XRPD technique, which is unable to reveal subtle structural differences for nano-sized and disordered materials.[59]

DR UV-Vis-NIR spectroscopy was applied to monitor the evolution of the electronic properties during the transition from the $MgCl_2$-6MeOH and $MgCl_2$-6EtOH precursors to the activated $MgCl_2$ (Figure 3). The spectra of the starting $MgCl_2$-6ROH adducts (spectra 1 in Figure 3a and b, respectively) show two main bands at ca. 31000 and 38500 cm^{-1}, which are assigned to charge-transfer (CT) transitions involving the Mg^{2+} centers and the ROH ligands, while the bands observed below 10000 cm^{-1} (very narrow) are the overtones and combinations of the vibrational modes of the ROH molecules. Upon dealcoholation, the bands below 10000 cm^{-1} progressively disappear, while the CT bands are gradually modified both in intensity and in position. In particular, a new intense absorption band gradually appears at ca. 42000 cm^{-1}, which is tentatively ascribed to the charge transfer transition from a Cl^- ligand to a highly uncoordinated Mg^{2+} center, in analogy to what reported by Zecchina et al. for defects on MgO.[86] A second envelope of bands is detectable in the final spectrum (spectrum 7) at 33000 and 23500 cm^{-1}, which are responsible for the goldenrod yellow color of the samples and are compatible with the presence of trapped electrons, i.e. color centers.[87] This phenomenon is more pronounced for the $MgCl_2$-$EtOH_{-250}$

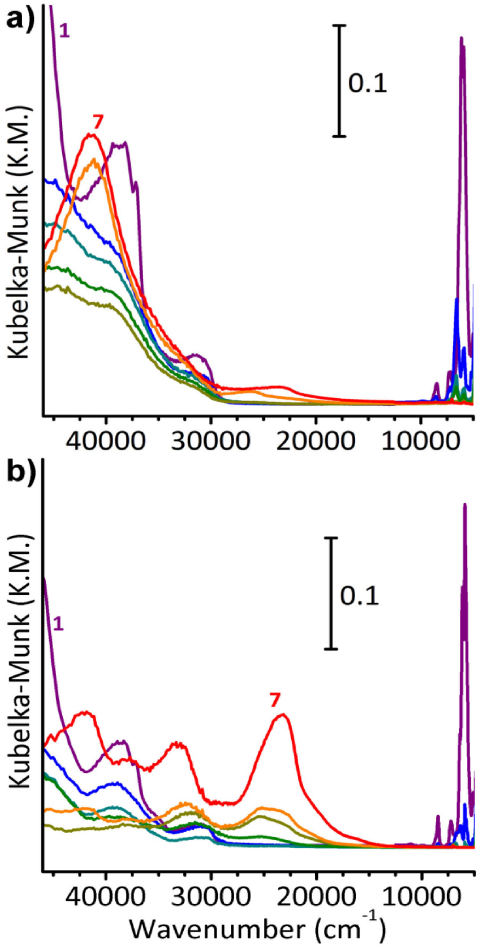

Figure 3. Evolution of the diffuse reflectance (DR) UV-Vis spectra upon dealcoholation of $MgCl_2$-6MeOH (part a) and $MgCl_2$-EtOH (part b), under N_2 flux (20 mL/min) at increasing temperatures (2 °C/min), from 25 to 250 °C. The color code is the same as in Figure 1 (25, 60, 90, 120, 150, 200 and 250 °C for $MgCl_2$-MeOH, and 25, 50, 80, 120, 170, 200 and 250 °C for $MgCl_2$-EtOH).

sample (Figure 3b). These bands are not affected by the successive adsorption of molecules (including H_2O), suggesting that the color centers are buried in the bulk of the $MgCl_2$ (and hence not relevant to the catalysis).

Finally, Figure 4 shows the evolution of the DRIFT spectra during the dealcoholation of $MgCl_2$-6ROH at increasing temperature. In the case of $MgCl_2$-6MeOH (Figure 4a), the initial spectrum is dominated by the absorption bands of the methanol molecules entangled within the material. The spectrum of liquid methanol (reported in Figure 4a for the sake of comparison) is characterized by the ν(OH) band at 3330 cm^{-1}, the asymmetric and symmetric ν(CH_3) at 2943 and 2832 cm^{-1}, the δ(CH_3) at 1450 cm^{-1}, the δ(OH) at 1420 cm^{-1}, $\delta_{rocking}$(OH) at 1115 cm^{-1}, the ν(C–O) at 1022 cm^{-1}, and a very weak and broad band at 2600–2500 cm^{-1} including several combinations of the bending and rocking modes.[88] In the ν(OH) region, the spectrum of $MgCl_2$-6MeOH is very similar to that of liquid methanol. This is in agreement with the NMR data reported by Butler et al., indicating that the MeOH molecules in the solvation shell of Mg halides are perturbed in a similar way as the MeOH molecules in the liquid phase.[89]

In the ν(CH_x) region, the bands due to the asymmetric and symmetric ν(CH_3) modes are more spaced to each other (at 2960 and 2795 cm^{-1}) because of the interaction with the Cl^- counterions, and three new bands are present at 2980, 2867 and 2750 cm^{-1}. The three bands are respectively assigned to the asymmetric and symmetric ν(CH_3) and to the overtone of the δ(CH_3) for methoxy ligands coordinated to the Mg^{2+}.[90,91]

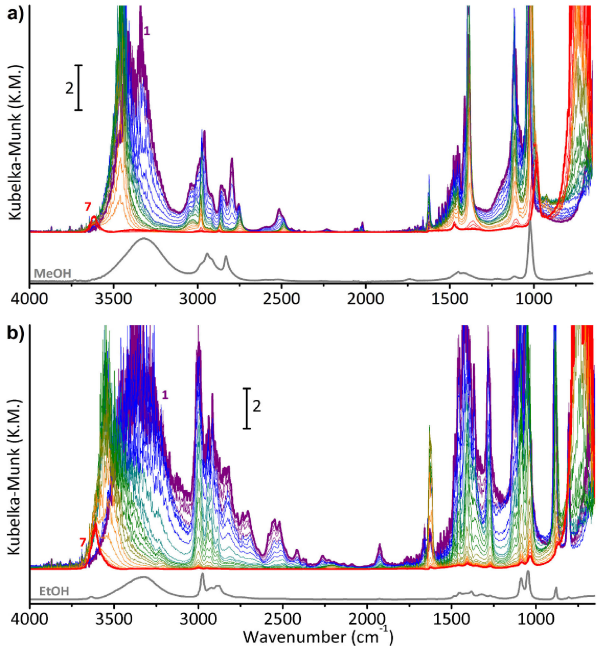

Figure 4. Evolution of the diffuse reflectance infrared Fourier transform (DRIFT) spectra upon dealcoholation of $MgCl_2$-6MeOH (part a) and $MgCl_2$-EtOH (part b), under N_2 flux (20 mL/min) at increasing temperatures (2 °C/min), from 25 to 250 °C. The color code is the same as in Figure 1 (25, 60, 90, 120, 150, 200 and 250 °C for $MgCl_2$-MeOH, and 25, 50, 80, 120, 170, 200 and 250 °C for $MgCl_2$-EtOH). Both sequences of DRIFT spectra are compared with the spectra of respective liquid alcohols collected in attenuated total reflectance (ATR) mode.

During the dealcoholation process, the ν(OH) band reduces in intensity and progressively shifts up-ward to ca. 3620 cm^{-1}, because of the continuous loss of the H-bonding interaction among the alcohol molecules in the coordination sphere of the Mg^{2+} ions. In the ν(CH_x) region, the spectra gradually simplify, and the bands associated to the methoxy species are the only ones remaining in the final spectrum, although with a very low intensity. As a matter of fact, spectrum 7 is characterized by a very low absorption in the whole spectral range (as expected, since neat $MgCl_2$ should be completely transparent in the Mid-IR region). The few residual bands indicate the persistence of a small number of alcohol-derived moieties, strongly bound to the $MgCl_2$. The most intense band (out-of-scale in DRIFT) is centered around 750 cm^{-1}, and indicates the formation of Mg–O covalent bonds. These results are in good agreement with the recent findings, which pointed out the formation of methoxy groups during the synthesis of methanol-shaped Ziegler-Natta catalysts through the thermal deprotonation of the outgoing MeOH molecules.[92] Finally, it should be also noted that a weak band at 1620 cm^{-1} starts growing during the first steps of the dealcoholation, but rapidly decreases at temperatures above 120 °C. This band is assigned to the δ(OH) vibrational mode of physisorbed water,[91] which derives from very small impurities in the N_2 flux despite the optimization of the experimental setup. This adventitious water cannot adsorb until the $MgCl_2$ surface is covered by the alcohol and is easily removed at temperatures above the boiling point.

An analogous sequence of DRIFT spectra was also observed upon dealcoholation of the $MgCl_2$-6EtOH adduct (Figure 4b). Also in this case the first spectrum is dominated by the spectroscopic manifestations of the pure alcohol, whereas the last spectrum presents only a few bands due to residual ethoxy byproducts, whose formation has already been assessed in literature.[66,93]

The whole set of experimental data discussed in this section converges in showing that the stepwise dealcoholation of the $MgCl_2$-6ROH adducts occurs through the formation of a large number of intermediate species (some of them crystalline) and following a series of side reactions often neglected in the specialized literature. The slightly different evolution of the two alcoholate precursors may explain the different properties of the produced $MgCl_2$, in terms of specific surface area, particles size and morphology.[58,59,94,95]

2.2. Genesis of Active Sites on $MgCl_2$

The reactions of the high surface area $MgCl_2$ with $TiCl_4$ and TEA, leading to the active Ziegler-Natta catalyst, were followed by *operando* DR UV-Vis and DRIFT spectroscopic techniques. Qualitatively, no significant differences are observed between the spectra collected on the sample derived from the $MgCl_2$-6MeOH and the spectra collected on the sample derived from the $MgCl_2$-6EtOH, indicating that the different precursors affect only the content and the distribution of the Ti centers, but not their intrinsic properties.

Upon dosage of a stoichiometric amount of $TiCl_4$ at 90 °C, two intense absorption bands at 42000 and 35500 cm^{-1} (with a well-defined shoulder at 28000 cm^{-1}) appear in the DR UV-Vis spectrum (spectrum 2 in Figure 5a). These bands are assigned to charge transfer transitions from the Cl ligands to the Ti metal centers of the newly formed $TiCl_x$ species. According to the Jorgensen rules on the optical electronegativities of transition metals and their ligands,[96,97] the band at 28000 cm^{-1} is univocally ascribed to 6-fold coordinated Ti^{4+} sites, while at higher wavenumbers also 4-fold coordinated Ti^{4+} sites give a contribution.[98] Interestingly, the band at 28000 cm^{-1} has a slightly slower dynamics than the other bands. This observation can be related to an initial step of physisorption of $TiCl_4$, which is arranged in tetrahedrons both in the liquid and vapor phases, followed by chemisorption in a more stable configuration, where Ti centers assume an octahedral geometry, as well established in the literature.[44,99–102] This spectral sequence is in agreement with the observations of Brambilla et al. for ball-milled $MgCl_2$-$TiCl_4$ complexes.[103] On the contrary, a few changes are observed upon titanation of $MgCl_{2\text{-}250}$ in the MIR region (spectrum 2 in Figure 5b). A slight decrease of the ν(OH) absorption band at around 3500 cm^{-1} indicates that $TiCl_4$ reacts with residual alcohol-derived species and/or with traces of adventitious H_2O on $MgCl_2$ surface. Such a reaction is also accompanied by the appearance of a very weak band at around 1100 cm^{-1} (clearly visible in the inset), which is attributed to the formation of Ti alkoxide byproducts.[104]

During the activation with TEA at 25 °C, an extensive absorption slowly appears in the DR UV-Vis spectra in the d-d region (from spectrum 2 to 3 in Figure 5a), showing the reduction of the Ti^{4+} centers to Ti^{3+}.[98] In particular, two bands are distinguishable at 21000 and 14500 cm^{-1}. These bands are quite broad and relatively intense (ca. 1 K.M. unit), despite the low concentration of Ti (1 wt%), suggesting that most of the Ti^{3+} sites are not isolated but rather aggregated into small clusters, as it was first proposed by Brant and Speca on the base of quantitative EPR measurements.[105,106] As a matter of fact, such a spectrum resembles those of the violet α and γ-$TiCl_3$,[16,98,107] which present two intense bands at 18300 and 13800 cm^{-1}. The latter band is ascribed to an intersite $^2T_{2g} \rightarrow {}^2E_g$ d-d transition involving two Ti^{3+} sites bridged by a Cl ligand, thus gaining intensity from the Cl→Ti CT transition at higher energy.[108] The slight blue-shift to higher wavenumbers of the $MgCl_{2\text{-}250}$/$TiCl_{4\text{-}90}$/TEA spectrum with respect to that of bulk $TiCl_3$ can be explained in terms of the smaller sizes of the $TiCl_x$ aggregates, but it is also compatible with the presence of alkyl ligands in the coordination sphere,[109] in accordance with the spectrochemical series of the ligands.[110] It is worth noticing that the DR UV-Vis spectra shown in Figure 5a neither exclude the presence of isolated Ti^{3+} sites (that should contribute at around 12000 cm^{-1},[108] or higher if alkylated,[111,112] but with a much weaker intensity), nor the presence of over-reduced Ti^{2+} sites (that should contribute in an extended spectral range, but with a very weak intensity).[113–115] We are tempted to exclude Ti over-reduction on account of the low amount of TEA used during the experiment (Al:Ti = 2:1),[116] but the co-presence of both isolated $TiCl_x$ species and Ti clusters, each one expressing a specific activity,[117] is plausible and cannot be discarded at all.

DRIFT spectra upon TEA dosage in Figure 5b are dominated by the absorption bands of the hexane solvent, but they are no more present in the final spectrum after flushing the cell with N_2 (spectrum 3). In that spectrum TEA dosage is testified by the appearance of some absorption bands in the ν(CH_x) (2950–2800 cm^{-1}) and δ(CH_x) (1500–1350 cm^{-1}) regions, which are related to the vibrational modes of the alkyl chains deriving from TEA. These bands are very similar to the fingerprints of pure TEA (inset in Figure 3b),[118] and account for the coexistence of alkylated $TiCl_xR_y$ species, AlR_xCl_y byproducts, and unreacted AlR_3, as already observed for other Ziegler-Natta catalysts.[119,120] Unfortunately, a clear distinction among all the different species could not be addressed here. Finally, a few changes are observed in the range between 1100 and 1000 cm^{-1}, likely associated to the reaction of TEA with the above mentioned Ti alkoxide species.

2.3. Ethylene Polymerization

The activity of the $MgCl_{2\text{-}250}$/$TiCl_{4\text{-}90}$/TEA catalyst towards ethylene polymerization was tested by contacting the catalyst

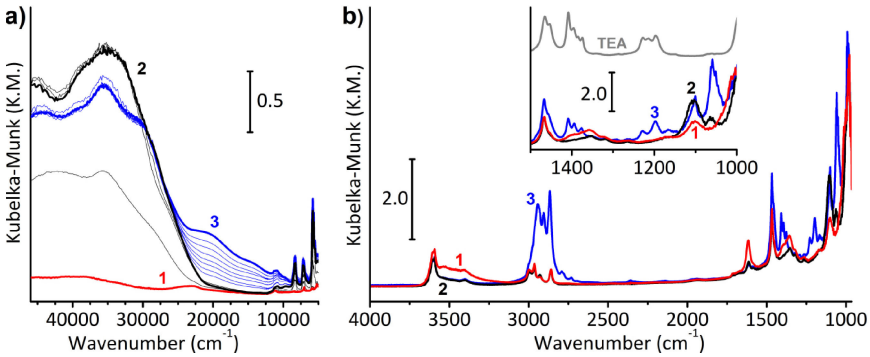

Figure 5. Evolution of the *operando* diffuse reflectance (DR) UV-Vis-NIR (Part a) and diffuse reflectance infrared Fourier transform (DRIFT) (Part b) spectra upon titanation of $MgCl_{2\text{-}250}$ at 90 °C with injections of hexane-diluted $TiCl_4$ in N_2 flux (from spectrum 1 to spectrum 2), and upon activation of $MgCl_{2\text{-}250}$/$TiCl_{4\text{-}90}$ at 25 °C with injections of hexane-diluted TEA in N_2 flux (from spectrum 2 to spectrum 3). Inset of part b shows a magnification of the DRIFT spectra in the 1500–1000 cm^{-1} region; the spectra are compared with the spectrum of liquid triethylaluminum (TEA) collected in attenuated total reflectance (ATR) mode.

with ethylene (20 mL/min, 25% of C_2H_4 in N_2) at room temperature and atmospheric pressure. Under these conditions, the catalyst is quickly submerged by a thick layer of polyethylene. This is well-evident in Figure 6, which shows the picture of the

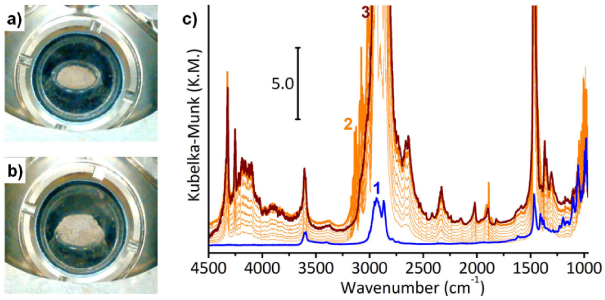

Figure 6. Parts a and b) Pictures of the $MgCl_{2\text{-}250}$/$TiCl_{4\text{-}90}$/TEA catalyst within the Harrick Praying Mantis diffuse reflectance infrared Fourier transform (DRIFT) cell before and after ethylene polymerization. Part c) Evolution of the *operando* FT-IR spectra upon ethylene polymerization (N_2:C_2H_4 = 75:25, 20 mL/min) on the $MgCl_{2\text{-}250}$/$TiCl_{4\text{-}90}$/TEA catalyst (from spectrum 1 to spectrum 2) and after flushing the cell with pure N_2 flux (spectrum 3). The spectra upon ethylene polymerization were collected every minute for 10 minutes.

sample in the DRIFT cell before (part a) and after (part b) ethylene polymerization (10 minutes). The powder enormously increases in size, up to overflow from the sample holder. As a consequence, no significant information can be achieved anymore by DR UV-Vis spectroscopy, because such a polymer coating changes the light scattering properties of the catalyst particles under study, shielding the catalytic sites from the incident light and negatively affecting the overall absorbance of the spectra, as clearly illustrated by Barzan et al. when studying ethylene polymerization on the Phillips catalyst.[26] The occurrence of ethylene polymerization is also clear by evaluating the evolution of the DRIFT spectra in Figure 6c, analogously to what recently observed on industrial catalysts.[112] After flushing the cell with pure N_2 to remove from the spectra the roto-vibrational contributions of gaseous ethylene (centered at 3105, 2990 and 1445 cm^{-1}), spectrum 3 in Figure 6c is dominated by the signals of growing polyethylene, that are the off-scale asymmetric and symmetric $\nu(CH_2)$ and $\delta(CH_2)$ modes (at around 2920, 2855 and 1470 cm^{-1}, respectively), and the very weak overtones and combinations (e.g., $\nu_{asym}(CH_2)+\delta(CH_2)$ and $\nu_{sym}(CH_2)+\delta(CH_2)$ at 4320 and 4250 cm^{-1}, respectively), further demonstrating the formation of polyethylene by the catalyst system under study.[121,122]

3. Conclusions

The individual steps for the synthesis of a Ziegler-Natta catalyst were successfully monitored, pointing out all the intermediate transitions that could not have been detected otherwise, but are crucial for the final composition of the catalyst. Although the adopted procedure is unusual for the industrial practice, where most of the reactions take place all at once within the reactor, some important remarks were achieved on the genesis of the Ziegler-Natta catalysts. The dealcoholation of $MgCl_2$-nMeOH and $MgCl_2$-nEtOH adducts to arrive at a high-surface area $MgCl_2$ evolves through a considerable number of intermediate phases (some of them found to be crystalline), resulting in the formation of alcohol-derived by-products strongly bound to the material. Such an observation substantiate the different properties reported in literature for $MgCl_2$ derived from different alcoholate precursors. Then, the titanation of the so formed $MgCl_2$ support material appears to be divided into two sequential steps, in which $TiCl_4$ is first physisorbed onto the surface and then strongly chemisorbed on $MgCl_2$. Finally, the activation of the pre-catalyst by triethylaluminum clearly causes the formation of Ti clusters through the partial aggregation of the surface $TiCl_x$ species, although the concurrent presence of isolated Ti centers cannot be discarded. The resulting Ziegler-Natta catalyst, synthesized through a surface science approach, presented a valuable activity towards ethylene polymerization, hence it can be considered as representative for industrial catalysts.

The reported data clearly demonstrate that *operando* spectroscopy allow appreciating transient details, that otherwise would not be revealed. Such information can be complementary with the fundamental studies under static conditions already present in literature, highlighting expediencies and criticalities intrinsic to the catalytic process, but which are often neglected. In this way it is possible to acquire a more complete knowledge of Ziegler-Natta catalysis.

Experimental Section

Materials Synthesis

Anhydrous $MgCl_2$ powder (≥99%), methanol (99.8%) and ethanol (≥99.8%), toluene (99.8%), hexane (95%), $TiCl_4$ (99.9%), and triethylaluminum (TEA, 93%) were used as received from Sigma-Aldrich. All the compounds were handled in a glove-box and treated under N_2 flux (>99.998%, Rivoira), in order to avoid possible contaminations. Solvents were dried under activated molecular sieves.

All experimental steps are summarized in Scheme 1 and described in detail in the following paragraphs.

The $MgCl_2$-nROH adducts were synthesized through an azeotropic distillation method (step a in Scheme 1), stirring for 3 h at 95 °C under inert atmosphere a solution of $MgCl_2$ in alcohol (either methanol or ethanol, 12 mL per gram of $MgCl_2$) and toluene, according to a procedure well established in the literature,[78,123] and in the same way as reported in previous works.[45,59] At the end of the process, the precipitation of the $MgCl_2$-nCH_3OH or $MgCl_2$-nCH_3CH_2OH powders occurred, in agreement with the $MgCl_2$ solubility models proposed by Zeng et al.[124]

The controlled dealcoholation of the $MgCl_2$-nROH adducts (step b) was achieved in N_2 flux (20 mL/min), heating the samples with a temperature ramp of 2 °C/min up to 250 °C, followed by 30 min of isotherm at the same temperature. The final temperature of this thermal treatment was chosen on the basis of the thermogravimetrical analysis (TGA), to assure the complete removal of all the

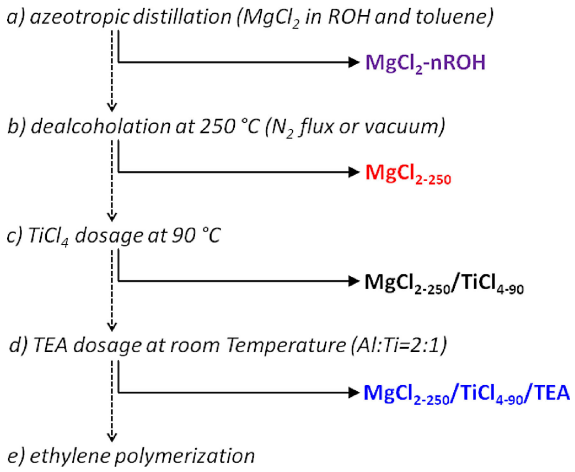

Scheme 1. Sequence of the experimental steps for the whole catalytic process under examination. All stages are labeled as in the main text, following the same color code in the next figures.

alcohol molecules. The activated high-surface area $MgCl_2$ will be referred to as $MgCl_{2\text{-}250}$.

For the titanation of activated $MgCl_2$ (step c), a stoichiometric amount of $TiCl_4$, necessary for achieving a final Ti content of 1 wt%, was diluted in hexane (50% v/v in hexane) and injected through a septum in the N_2 flux (20 mL/min). Then the $TiCl_4$ vapors reach with the activated $MgCl_2$ at 90 °C. The employed setup is similar to that described in previous work.[27] The final amount of titanium that is grafted on $MgCl_2$ with this procedure is close to 1.0 wt%, as determined by ICP analysis.[45] The so formed pre-catalysts will hereafter be referred to as $MgCl_{2\text{-}250}/TiCl_{4\text{-}90}$.

The activation of the $MgCl_{2\text{-}250}/TiCl_{4\text{-}90}$ pre-catalyst (step d) was accomplished by using a diluted solution of TEA (1.25 M in hexane), attaining an average Ti:Al stoichiometry of 1:2, with respect to the total $TiCl_4$ injected. TEA was dosed at room temperature, following the same procedure described for $TiCl_4$ dosage. The resulting active catalyst will be referred to as $MgCl_{2\text{-}250}/TiCl_{4\text{-}90}$/TEA.

Both $TiCl_4$ and TEA dosages are followed by a mild washing of the catalyst by injecting some pure solvent into the N_2 flux through the sample.

Ethylene polymerization (step e) was performed flowing through the measurement cell at 20 mL/min a 75:25 mixture of N_2 and C_2H_4 (>99.9%, Linde), at room temperature and atmospheric pressure.

Materials Characterization and Testing

Thermogravimetric analysis (TGA) measurements during the $MgCl_2$-nROH dealcoholation were performed with a TA Q600 instrument at a heating rate of 2 °C/min in a temperature range between 30 and 300 °C, under N_2 flux (50 mL/min). *Operando* X-ray powder diffraction (XRPD) measurements were performed using a PANalytical X'Pert diffractometer (Cu K_α radiation), inserting a flat sample (Bragg-Brentano geometry) into an Anton Paar XRK 900 reactor chamber equipped with a hot stage and gas fluxing system. A sequence of isothermal measurements was performed in the range 25–250 °C, following the temperature steps derived from the TGA analysis (the heating rate between each isotherm was 2 °C/min). *Operando* FT-IR spectra were collected in diffuse reflectance mode (DRIFT) with a spectral resolution of 2 cm^{-1} with a Perkin-Elmer 2000 spectrometer equipped with a DTGS detector. The samples were positioned inside a Harrick Praying Mantis DRIFT accessory equipped with ZnS windows, connected with a gas flow system. The UV-Vis-NIR spectra were collected in diffuse reflectance (DR) mode using a Varian Cary5000 spectrophotometer, equipped with a perfectly white reflectance sphere. The samples were placed inside a quartz cell with an optical quartz window ("Suprasil"). The spectra were collected in reflectance and successively converted into Kubelka-Munk units.

Conflict of Interest

The authors declare no conflict of interest.

Keywords: catalysis · ethylene polymerization · operando spectroscopy · X-ray diffraction · Ziegler-Natta catalysts

[1] H. Topsøe, *J. Catal.* **2003**, *216*, 155.
[2] B. M. Weckhuysen, *Phys. Chem. Chem. Phys.* **2003**, *5*, 4351.
[3] S. J. Tinnemans, J. G. Mesu, K. Kervinen, T. Visser, T. A. Nijhuis, A. M. Beale, D. E. Keller, A. M. J. van der Eerden, B. M. Weckhuysen, *Catal. Today* **2006**, *113*, 3.
[4] M. A. Bañares, *Catal. Today* **2005**, *100*, 71.
[5] M. A. Bañares, *Adv. Mater.* **2011**, *23*, 5293.
[6] C. Otero Areán, B. M. Weckhuysen, A. Zecchina, *Phys. Chem. Chem. Phys.* **2012**, *14*, 2125.
[7] Y. Zhang, D. Fu, X. Xu, Y. Sheng, J. Xu, Y. Han, *Curr. Opin. Chem. Eng.* **2016**, *12*, 1.
[8] A. Chakrabarti, M. E. Ford, D. Gregory, R. Hu, C. J. Keturakis, S. Lwin, Y. Tang, Z. Yang, M. Zhu, M. A. Bañares, I. E. Wachs, *Catal. Today* **2017**, *283*, 27.
[9] J. Scalbert, C. Daniel, Y. Schuurman, C. Thomas, F. C. Meunier, *J. Catal.* **2014**, *318*, 61.
[10] C. H. Choi, C. Baldizzone, J.-P. Grote, A. K. Schuppert, F. Jaouen, K. J. J. Mayrhofer, *Angew. Chem. Int. Ed.* **2015**, *54*, 12753.
[11] J. Song, Y. Wang, E. D. Walter, N. M. Washton, D. Mei, L. Kovarik, M. H. Engelhard, S. Prodinger, Y. Wang, C. H. F. Peden, F. Gao, *ACS Catal.* **2017**, *7*, 8214.
[12] E. Sagel, in *Foro Pemex*, IHS Inc, Mexico City, **2012**.
[13] H. A. Wittcoff, B. G. Reuben, J. S. Plotkin, *Industrial Organic Chemicals: Third Edition*, John Wiley and Sons, **2013**.
[14] *Market Report: Global Catalyst Market*, 3rd ed., Acmite Market Intelligence, Ratingen, Germany, **2015**.
[15] T. J. Hutley, M. Ouederni, in *Polyolefin Compounds and materials* (Eds.: M. A.-A. AlMa'adeed, I. Krupa), Springer, Switzerland, **2016**, pp. 13.
[16] E. Groppo, K. Seenivasan, C. Barzan, *Catal. Sci. Technol.* **2013**, *3*, 858.
[17] P. Corradini, G. Guerra, L. Cavallo, *Acc. Chem. Res.* **2004**, *37*, 231.
[18] A. Correa, R. Credendino, J. T. M. Pater, G. Morini, L. Cavallo, *Macromolecules* **2012**, *45*, 3695.
[19] E. Groppo, E. Gallo, K. Seenivasan, A. Sommazzi, S. Bordiga, P. Glatzel, R. Van Silfhout, A. Kachatkou, W. Bras, C. Lamberti, *ChemCatChem* **2015**, *7*, 1432.
[20] E. Morra, E. Giamello, S. Van Doorslaer, G. Antinucci, M. D'Amore, V. Busico, M. Chiesa, *Angew. Chem. Int. Ed.* **2015**, *54*, 4857.
[21] A. Vittoria, A. Meppelder, N. Friederichs, V. Busico, R. Cipullo, *ACS Catal.* **2017**, *7*, 4509.
[22] C. Copéret, F. Allouche, K. W. Chang, M. Conley, M. F. Delley, A. Fedorov, I. Moroz, V. Mougel, M. Pucino, K. Searles, K. Yamamoto, P. Zhizhko, *Angew. Chem. Int. Ed.* **2017**.
[23] T. Taniike, M. Terano, *J. Catal.* **2012**, *293*, 39.
[24] V. Busico, R. Cipullo, A. Mingione, L. Rongo, *Ind. Eng. Chem. Res.* **2016**, *55*, 2686.
[25] E. G. Derouane, F. Lemos, A. Corma, F. R. Ribeiro, *Combinatorial catalysis and high throughput catalyst design and testing, Vol. 560*, Springer Science & Business Media, **2012**.
[26] C. Barzan, A. Piovano, L. Braglia, G. A. Martino, C. Lamberti, S. Bordiga, E. Groppo, *J. Am. Chem. Soc.* **2017**, *139*, 17064.
[27] D. Cicmil, J. Meeuwissen, A. Vantomme, B. M. Weckhuysen, *ChemCatChem* **2016**, *8*, 1937.

[28] D. Cicmil, I. K. Van Ravenhorst, J. Meeuwissen, A. Vantomme, B. M. Weckhuysen, *Catal. Sci. Tech.* **2016**, *6*, 731.
[29] E. Albizzati, U. Giannini, G. Collina, L. Noristi, L. Resconi, in *Polypropylene Handbook* (Ed.: E. P. J. Moore), Hanser-Gardner Publications, Cincinnati (Ohio, USA), **1996**.
[30] P. Galli, G. Vecellio, *Prog. Polym. Sci.* **2001**, *26*, 1287.
[31] E. P. Moore, *The Rebirth of Polypropylene: Supported Catalysts: how the People of the Montedison Laboratories Revolutionized the PP Industry*, Hanser Pub., New York, **1998**.
[32] R. Zannetti, C. Marega, A. Marigo, A. Martorana, *J. Polym. Sci., Part B: Polym. Phys.* **1988**, *26*, 2399.
[33] N. Kashiwa, *J. Polym. Sci., Part A: Polym. Chem.* **2004**, *42*, 1.
[34] U. Müller, *Inorganic structural chemistry*, John Wiley & Sons, Chichester (UK), **2006**.
[35] M. Kakugo, T. Miyatake, Y. Naito, K. Mizunuma, *Macromolecules* **1988**, *21*, 314.
[36] M. Kioka, H. Makio, A. Mizuno, N. Kashiwa, *Polym.* **1994**, *35*, 580.
[37] V. Busico, in *Polyolefins: 50 years after Ziegler and Natta I, Vol. 257* (Ed.: W. Kaminsky), Springer, Berlin, **2013**, pp. 37.
[38] J. C. Chadwick, F. van der Burgt, S. Rastogi, V. Busico, R. Cipullo, G. Talarico, J. J. R. Heere, *Macromolecules* **2004**, *37*, 9722.
[39] Y. P. Chen, Z. Q. Fan, J. H. Liao, S. Q. Liao, *J. Appl. Polym. Sci.* **2006**, *102*, 1768.
[40] L. Noristi, E. Marchetti, G. Baruzzi, P. Sgarzi, *J. Polym. Sci., Part A: Polym. Chem.* **1994**, *32*, 3047.
[41] T. F. McKenna, J. B. P. Soares, *Chem. Eng. Sci.* **2001**, *56*, 3931.
[42] K. Soga, T. Shiono, Y. Doi, *Polym. Bull.* **1983**, *10*, 168.
[43] F. J. Gómez, R. M. Waymouth, *Science* **2002**, *295*, 635.
[44] M. D'Amore, R. Credendino, P. H. M. Budzelaar, M. Causá, V. Busico, *J. Catal.* **2012**, *286*, 103–110.
[45] M. D'Amore, K. S. Thushara, A. Piovano, M. Causà, S. Bordiga, E. Groppo, *ACS Catal.* **2016**, *6*, 5786.
[46] D. N. Taveira Magalhães, O. Do Coutto Filho, F. M. B. Coutinho, *Eur. Polym. J.* **1991**, *27*, 1093.
[47] F. J. Karol, *Catal. Rev.: Sci. Eng.* **1984**, *26*, 557.
[48] F. J. Karol, K. J. Cann, B. E. Wagner, in *Transition Metals and Organometallics as Catalysts for Olefin Polymerization* (Eds.: W. Kaminsky, H. Sinn), Springer, Berlin, **1988**, pp. 149.
[49] Y. V. Kissin, *Alkene Polymerization Reactions with Transition Metal Catalysts, Vol. 173*, Elsevier, Amsterdam, **2008**.
[50] T. E. Nowlin, R. I. Mink, Y. V. Kissin, in *Transition Metal Polymerization Catalysts* (Eds.: R. Hoff, R. T. Mathers), John Wiley & Sons, Hoboken (New Jersey), **2009**, pp. 131.
[51] T. E. Nowlin, *Business and Technology of the Global Polyethylene Industry*, Wiley-Scrivener, New York, **2014**.
[52] V. H. Nissinen, I. O. Koshevoy, T. T. Pakkanen, *Dalton Trans.* **2017**, *46*, 4452.
[53] S. Pirinen, K. Jayaratne, P. Denifl, T. T. Pakkanen, *J. Mol. Catal. A: Chem.* **2014**, *395*, 434.
[54] S. Pirinen, T. T. Pakkanen, *J. Mol. Catal. A: Chem.* **2015**, *398*, 177.
[55] N. Friederichs, R. Gerlofsma, WO2009112254, **2009**.
[56] E. Puhakka, T. T. Pakkanen, T. A. Pakkanen, *J. Phys. Chem. A* **1997**, *101*, 6063.
[57] A. Andoni, J. C. Chadwick, H. J. W. Niemantsverdriet, P. C. Thune, *Macromol. Rapid Commun.* **2007**, *28*, 1466.
[58] A. Andoni, J. C. Chadwick, H. J. W. Niemantsverdriet, P. C. Thune, *J. Catal.* **2008**, *257*, 81.
[59] K. S. Thushara, M. D'Amore, A. Piovano, S. Bordiga, E. Groppo, *ChemCatChem* **2017**, *9*, 1782.
[60] V. H. Nissinen, M. Linnolahti, T. T. Pakkanen, *J. Phys. Chem. C* **2016**, *120*, 21505.
[61] A. Andoni, J. C. Chadwick, J. W. Niemantsverdriet, P. C. Thune, *Catal. Lett.* **2009**, *130*, 278.
[62] V. Di Noto, R. Zannetti, M. Vivani, C. Marega, A. Marigo, S. Bresadola, *Makromol. Chem.* **1992**, *193*, 1653.
[63] C. R. Tewell, F. Malizia, J. W. Ager III, G. A. Somorjai, *J. Phys. Chem. B* **2002**, *106*, 2946.
[64] Z. Y. Ye, L. Wang, L. F. Feng, X. P. Gu, H. H. Chen, P. Y. Zhang, J. Pan, S. Jiang, L. X. Feng, *J. Polym. Sci., Part A: Polym. Chem.* **2002**, *40*, 3112.
[65] P. Sozzani, S. Bracco, A. Comotti, R. Simonutti, I. Camurati, *J. Am. Chem. Soc.* **2003**, *125*, 12881.
[66] V. D'Anna, S. Norsic, D. Gajan, K. Sanders, A. J. Pell, A. Lesage, V. Monteil, C. Copéret, G. Pintacuda, P. Sautet, *J. Phys. Chem. C* **2016**, *120*, 18075.
[67] J. C. J. Bart, W. Roovers, *J. Mater. Sci.* **1995**, *30*, 2809.
[68] E. Jalali Dil, S. Pourmahdian, M. Vatankhah, F. A. Taromi, *Polym. Bull.* **2010**, *64*, 445.
[69] E. Y. X. Chen, T. J. Marks, *Chem. Rev.* **2000**, *100*, 1391.
[70] D. V. Stukalov, V. A. Zakharov, *J. Phys. Chem. C* **2009**, *113*, 21376.
[71] H. Fuhrmann, W. Herrmann, *Macromol. Chem. Phys.* **1994**, *195*, 3509.
[72] K. Soga, S. I. Chen, R. Ohnishi, *Polym. Bull.* **1982**, *8*, 473.
[73] J. C. W. Chien, S. Weber, Y. Hu, *J. Polym. Sci. A* **1989**, *27*, 1499.
[74] S. H. Kim, G. A. Somorjai, *Proc. Nat. Acad. Sci. U. S. A.* **2006**, *103*, 15289.
[75] Y. V. Kissin, *J. Catal.* **2012**, *292*, 188.
[76] N. Bahri-Laleh, A. Correa, S. Mehdipour-Ataei, H. Arabi, M. N. Haghighi, G. Zohuri, L. Cavallo, *Macromolecules* **2011**, *44*, 778.
[77] T. Taniike, T. Funako, M. Terano, *J. Catal.* **2014**, *311*, 33.
[78] E. S. Gnanakumar, R. R. Gowda, S. Kunjir, T. G. Ajithkumar, P. R. Rajamohanan, D. Chakraborty, C. S. Gopinath, *ACS Catal.* **2013**, *3*, 303.
[79] T. Radnai, E. Kálmán, K. Pollmer, *Z. Naturforsch. A* **1984**, *39*, 464.
[80] Y. Tamura, E. Spohr, K. Heinzinger, G. Pálinkás, I. Bakó, *Ber. Bunsenges. Phys. Chem.* **1992**, *96*, 147.
[81] S. Halut-Desportes, M. Philoche-Levisalles, *Acta Cryst. B* **1978**, *34*, 432.
[82] H. S. Cho, W. Y. Lee, *J. Mol. Catal. A Chem.* **2003**, *191*, 155.
[83] F. Auriemma, C. De Rosa, *Chem. Mater.* **2007**, *19*, 5803.
[84] F. Auriemma, C. De Rosa, *J. Appl. Cryst.* **2008**, *41*, 68.
[85] M. Chang, X. Liu, P. J. Nelson, G. R. Munzing, T. A. Gegan, Y. V. Kissin, *J. Catal.* **2006**, *239*, 347.
[86] A. Zecchina, M. G. Lofthouse, F. S. Stone, *J. Chem. Soc., Faraday Trans. 1* **1975**, *71*, 1476.
[87] S. Kinno, R. Onaka, *J. Phys. Soc. Jpn.* **1983**, *52*, 267.
[88] M. Falk, E. Whalley, *J. Chem. Phys.* **1961**, *34*, 1554.
[89] R. N. Butler, J. Davies, M. C. R. Symons, *Trans. Faraday Soc.* **1970**, *66*, 2426.
[90] H. S. Jung, J.-K. Lee, J.-Y. Kim, K. S. Hong, *J. Colloid Interface Sci.* **2003**, *259*, 127.
[91] A. A. Rywak, J. M. Burlitch, T. M. Loehr, *Chem. Mater.* **1995**, *7*, 2028.
[92] H. S. Cho, W. Y. Lee, *Korean J. Chem. Eng.* **2002**, *19*, 557.
[93] E. Grau, A. Lesage, S. Norsic, C. Copéret, V. Monteil, P. Sautet, *ACS Catal.* **2013**, *3*, 52.
[94] K. S. Thushara, E. S. Gnanakumar, R. Mathew, T. G. Ajithkumar, P. R. Rajamohanan, S. Bhaduri, C. S. Gopinath, *Dalton Trans.* **2012**, *41*, 11311.
[95] E. Redzic, T. Garoff, C. C. Mardare, M. List, G. Hesser, L. Mayrhofer, A. W. Hassel, C. Paulik, *Iran. Polym. J.* **2016**, *25*, 321.
[96] C. K. Jorgensen, in *Orbitals in Atoms and Molecules*, Academic Press, London and New York, **1962**, pp. 80.
[97] C. K. Jorgensen, *Progr. Inorg. Chem.* **1970**, *12*, 101.
[98] K. Seenivasan, A. Sommazzi, F. Bonino, S. Bordiga, E. Groppo, *Chem. Eur. J* **2011**, *17*, 8648.
[99] P. Corradini, V. Barone, R. Fusco, G. Guerra, *Gazz. Chim. Ital.* **1983**, *113*, 601.
[100] V. Busico, P. Corradini, L. De Martino, A. Proto, V. Savino, E. Albizzati, *Makromol. Chem.* **1985**, *186*, 1279.
[101] T. Taniike, M. Terano, *Macromol. Rapid Commun.* **2008**, *29*, 1472.
[102] D. V. Stukalov, I. L. Zilberberg, V. A. Zakharov, *Macromolecules* **2009**, *42*, 8165.
[103] L. Brambilla, G. Zerbi, F. Piemontesi, S. Nascetti, G. Morini, *J. Mol. Catal. A-Chem.* **2007**, *263*, 103.
[104] R. Urlaub, U. Posset, R. Thull, *J. Non-Cryst. Solids* **2000**, *265*, 276.
[105] P. Brant, A. N. Speca, *Macromolecules* **1987**, *20*, 2740.
[106] P. Brant, A. N. Speca, D. C. Johnston, *J. Catal.* **1988**, *113*, 250.
[107] I. Pollini, *Solid State Commun.* **1983**, *47*, 403.
[108] R. J. H. Clark, *J. Chem. Soc.* **1964**, *0*, 417.
[109] W. W. Lukens, M. R. Smith, R. A. Andersen, *J. Am. Chem. Soc.* **1996**, *118*, 1719.
[110] P. Atkins, T. Overton, J. Rourke, M. Weller, F. Armstrong, *Shriver and Atkins' Inorganic Chemistry*, 5th ed., Oxford University Press, New York, **2010**.
[111] A. Piovano, K. S. Thushara, E. Morra, M. Chiesa, E. Groppo, *Angew. Chem. Int. Ed.* **2016**, *55*, 11203.
[112] P. Pletcher, A. Welle, A. Vantomme, B. M. Weckhuysen, *J. Catal.* **2018**, *363*, 128.
[113] C. W. DeKock, D. M. Gruen, *J. Chem. Phys.* **1966**, *44*, 4387.
[114] M. A. Araya, F. A. Cotton, J. H. Matonic, C. A. Murillo, *Inorg. Chem.* **1995**, *34*, 5424.
[115] U. Kölle, P. Kölle, *Angew. Chem. Int. Ed.* **2003**, *42*, 4540.
[116] J. C. W. Chien, J. Wu, C. Kuo, *J. Polym. Sci. Polym. Chem. Ed.* **1982**, *20*, 2019.
[117] S. Takahashi, T. Wada, T. Taniike, M. Terano, *Catalysts* **2013**, *3*, 137.
[118] S. Kvisle, E. Rytter, *Spectrochim. Acta A* **1984**, *40*, 939.

[119] A. Piovano, G. A. Martino, C. Barzan, *Rend. Fis. Acc. Lincei* **2017**, *28*, 43.
[120] A. Piovano, E. Morra, M. Chiesa, E. Groppo, *ACS Catal.* **2017**, *7*, 4915.
[121] S. Krimm, C. Y. Liang, G. B. B. M. Sutherland, *J. Chem. Phys.* **1956**, *25*, 549.
[122] J. R. Nielsen, A. H. Woollett, *J. Chem. Phys.* **1957**, *26*, 1391.
[123] K. S. Thushara, E. S. Gnanakumar, R. Mathew, R. K. Jha, T. G. Ajithkumar, P. R. Rajamohanan, K. Sarma, S. Padmanabhan, S. Bhaduri, C. S. Gopinath, *J.Phys.Chem.C* **2011**, *115*, 1952.
[124] L. Zeng, Z. Li, X. Wang, *J. Chem. Eng. Data* **2016**, *61*, 797.

Manuscript received: June 20, 2018
Version of record online: August 3, 2018